Curvilinear Structure Enhancement and Detection in Geophysical Images

Costas Panagiotakis, Eleni Kokinou, and Apostolos Sarris

***Abstract*—In this paper, we propose a method for automatic enhancement and identification of partial curvilinear structures. The accurate identification of line structures in geophysical images plays an important role in geophysical interpretation and the detection of subsurface structures. The method was applied on geophysical images in an effort to recognize the linear patterns of subsurface architectural structures that exist in archaeological sites. To our knowledge, the problem of identification of curvilinear structures in geophysical images for archaeological sites is faced for the first time. The method efficiently combines a rotation- and scale-invariant filter and a pixel-labeling method, providing a robust enhancement and detection of mostly line structures in 2-D grayscale images, respectively. Experimental results on real and synthetic images and comparison with existing methods in the literature indicated the reliable performance of the proposed scheme.**

***Index Terms*—Filtering, geophysical prospection, image analysis, rotation invariant, scale invariant.**

I. Introduction

THE automatic enhancement and detection of structures on real and complex 2-D images are important tasks on various applications of computer vision, medical analysis, and geosciences. In many of the above applications, the most fundamental feature of image understanding is the recognition of line structures in 2-D images, since line segments occur in various natural and synthetic objects. Upon the identification of the line segments, features can be better delineated.

One of the most widely used methods to solve the line detection problem in binary or grayscale images is the Hough transform [1], [2]. According to Hough transform, the detection of line segments is reduced to the detection of the peaks in a voting parameter space. This space is initially estimated by the voting of each original image point to all points in the parameter space that could have possibly produced the image point. Moreover, Hough Transform has been used to detect more complicated shapes like circle [3] and ellipses [4]. However, Hough Transform is difficult to be tuned due to the discretization of the continuous parameter space and due to the determination of the neighbor size that is used for peak estimation. Thus, in many cases, the estimated results are strongly associated to the input parameters.

In [5], curvilinear structures are enhanced by a nonlinear combination of linear filters. The filters are applied in different scales and orientations. The method has been successfully applied in 2-D and 3-D images. In [6], a scheme for the reconstruction of curvilinear structure regions based on skeleton extraction and skeletal segment classification is proposed. The skeleton is extracted from the Euclidean distance map that is constructed based on the edge map of an input image. Other techniques use Gabor filters [7] for estimation of image features. Gabor filter responses are characterized by orientation and spatial frequency selection. The estimated features have been used in the past to detect various complicated image structures like faces [8], textures [9], and characters [10].

Matching filters approaches [11], [12] convolve the image with multiple matched filters for the extraction of objects of interest, vessel contours in the vessel extraction domain. Matching filters procedure is usually followed with some other image processing operations like thresholding and then connected component analysis to get the final vessel contours. Hoover *et al.* [13] combine local and region-based properties to segment blood vessels in retinal images. Their method examines the image of a matched filter response (MFR) in pieces and applies thresholding using a probing technique. The probing technique classifies pixels in an area of the MFR as vessels and non-vessels by iteratively decreasing the threshold.

Tensor voting methods, which associate a tensor field with each edge pixel, are promising methods for contour detection in images [14]. These methods are based on saliency maps that are obtained by iteratively increasing the strength of those edges which have collinear edges in their immediate surrounding, and by reducing the strength of edges that are surrounded by random patterns. Alternatively, Gestalt theory concerns the ability of human observers to group visual stimuli which share certain common characteristics [15], [16]. In [15] and [16], two Gestalt-theory-based methods for contour detection have been proposed. In [15], the grouping algorithm is embedded in a multithreshold scheme which, at each threshold level, removes small groups of edges and recovers missing contours by means of a generalized reconstruction from markers. Similarly, in [16], a local grouping rule derived directly from the co-occurrence

Manuscript received May 28, 2010; revised September 5, 2010 and December 6, 2010; accepted December 15, 2010. Date of publication January 30, 2011; date of current version May 20, 2011. This work was supported in part by the Institute for Mediterranean Studies-FORTH.

C. Panagiotakis is with the Department of Commerce and Marketing, Technological Educational Institute Crete, Ierapetra 72200, Greece and also with the Department of Computer Science, University of Crete, 71409 Heraklion, Greece (e-mail: cpanag@csd.uoc.gr).

E. Kokinou is with the Laboratory of Geophysics and Seismology, Department of Natural Resources and Environment, Technological Educational Institute Crete, Chalepa, Chania, 73133 Crete, Greece (e-mail: ekokinou@chania.teicrete.gr).

A. Sarris is with the Laboratory of Geophysical-Satellite Remote Sensing & Archaeo-enviroment, Institute for Mediterranean Studies, Foundation for Research and Technology-Hellas, Rethymnon 74100 Crete, Greece (e-mail: asaris@ret.forthnet.gr).

Color versions of one or more of the figures in this paper are available online at http://ieeexplore.ieee.org.

Digital Object Identifier 10.1109/TGRS.2010.2102042

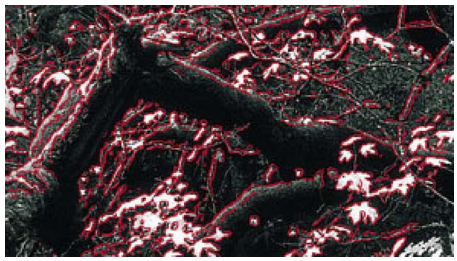

Fig. 1. Contour detection (red pixels) using a Gestalt-theory-based method in real image [16].

statistics is used, in combination with an integration rule that links the locally grouped contour elements into longer contours. A disadvantage of these methods is the high computational cost. Moreover, they need postprocessing to recognize the patterns of subsurface architectural structures since these contour detection methods will detect two "parallel" contours (pattern boundaries) for each pattern. Fig. 1 presents the application of Gestalt theory on a natural grayscale image. The detected contours are colored with red color.

The main contribution of this research is that it faces the problem of identification of curvilinear structures in geophysical images for archaeological sites, which is faced for the first time (to our knowledge). Concerning the proposed methodology, instead of using Gabor filters for feature estimation and high-computational-cost methods with postprocessing schemes, a line model filter that is applied into different scales and orientations is proposed, aiming toward the detection of lines of different widths and directions, respectively. The proposed method can be classified into matching filters techniques [11]. Then, the image of maximum values of the filter responses is estimated, providing an enhancement of invariant to rotation and scaling curvilinear structures. This procedure is similar to the Hough Transform methodology, where the peaks in voting parameter space are selected. Finally, a pixel-labeling method is applied, yielding the identification of partial curvilinear structures. The above method was employed on different images produced by geophysical measurements in archaeological sites, where a number of linear subsurface structures were suggested. In an earlier work of ours presented in [12], we have proposed a method for automatic enhancement of partial curvilinear structures on geophysical images. The current work focuses on automatic detection and enhancement, improving the preliminary results by introducing new filters models and the pixel-labeling algorithm.

The rest of the paper is organized as follows. Section II describes the geophysical image interpretation and the problem of relic recognition in archaeological sites. Section III presents the proposed scheme. Experimental results and comparisons are given in Section IV. Finally, conclusions are provided in Section V.

II. Geophysical Image Interpretation

Interpretation of 2-D geophysical images comprises the final and most important step of geophysical processing. Interpretation of the images depends mainly on the clarity of the images and on interpreter's experience and very few schemes

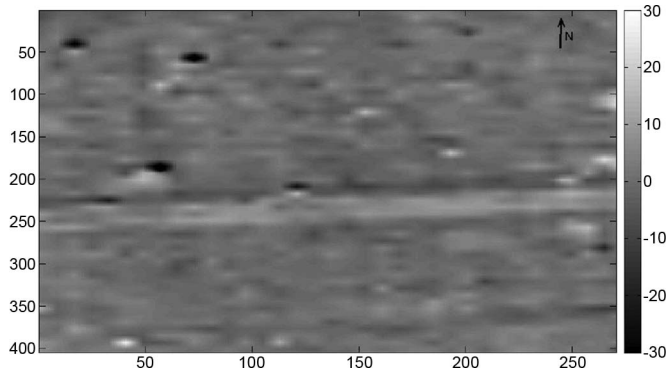

Fig. 2. Example of a geophysical image produced through a magnetic survey (measurements of vertical magnetic gradient, nT/m) at ancient Lefkada (Ionian Sea, Greece).

have been proposed for the automatic feature detection and extraction. These schemes mainly concern horizon tracking across discontinuities in 2-D and 3-D seismic data and image de-noising attempts [17]–[19].

With the fast advances in computing technology, there has been considerable and increasing interest in the development of automatic geophysical interpretation and understanding methodologies. Image processing and analysis techniques offer the means to acquire digital information, at different scales quickly and efficiently. The development of an efficient and effective computer-based approach for the automated geophysical image interpretation would allow the selection of more details in subsurface structures and the reduction of misinterpretation.

Shallow-depth geophysical prospection suffers from the influence of anthropogenic interventions and activities, both on the surface and below it, creating various difficulties in the presentation and interpretation of the results. For this reason, multiple geophysical techniques are preferably employed since their complementary measurements offer a better insight about the subsurface of the archaeological sites. The combined image constructed from these data, through different graphics and processing techniques, makes it easier to detect the location of the relics and visualize their extent within the subsurface. Still, the interpretation of the geophysical data is a difficult task since measurements are masked by cultural noise originated by the diachronic usage of the landscape or the modern agricultural or construction activities in an area of interest. As a result of the above processes, the image resulting by the interpolation of the geophysical measurements is often of poor quality, containing high percentages of random or systematic noise which hinder the valuable information related to the subsurface targets.

The noise in geophysical data has usually high-frequency content and characteristic frequencies depending on the causing sources; while in many cases, it is distributed across all spatial scales (see Fig. 2).

III. Proposed Scheme

In this section, the proposed methodology is described (see Fig. 3). First, noise reduction is performed. Next, the multiple filtering provides an enhancement of curvilinear structures. Finally, a pixel-labeling method provides the detection of curvilinear structures.

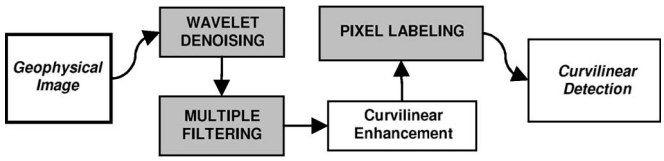

Fig. 3. Scheme of the proposed system architecture.

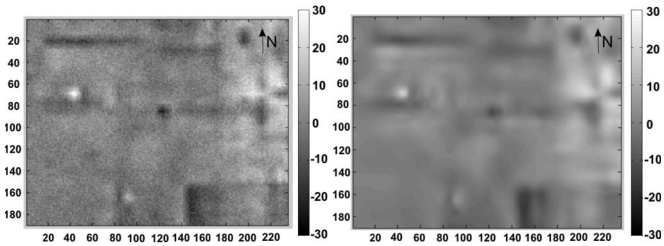

Fig. 4. (a) Original image and the (b) result of Wavelet de-noising filter [20]. The particular image originated by a magnetic survey at the site of ancient Sikyon in Peloponnese, Greece.

A. Noise Reduction

As it was mentioned in the previous section, a given geophysical image contains cultural noise, difficult to be modeled, originated by the diachronic usage of the landscape or the modern agricultural or construction activities. Therefore, in order to smoothen the noise of the image, the first step of the proposed scheme consists of a noise reduction module.

Wavelet decomposition is effective in decoupling the high-order statistical features of natural images. In addition, it shares some basic properties of neural responses in the primary visual cortex of mammals which are presumably adapted to represent efficiently the visually relevant features of images. For this reason, wavelet decomposition has been successfully applied on image [20], [21] or geophysical data [22], [23] denoising schemes.

In this research, denoising is performed via wavelet thresholding method [20]. It has been shown that wavelet thresholding schemes for denoising have near-optimal properties in the minimax sense and perform well in simulation studies of 1-D curve estimation. Wavelet thresholding method was implemented by Matlab, using an undecimated representation with four scales based on the minimum-phase Daubechies eight-tap wavelet filter. Fig. 4 illustrates a result of the proposed de-noising method. This image de-noising algorithm uses soft thresholding to provide smoothness and deter edge preservation at the same time. Hereafter, $\mathbf{I}$ and $\mathbf{I_d}$ denote the original and denoising images correspondingly.

B. Filter Model

In this section, the proposed filter model is presented. The filtering task aims toward the enhancement of curvilinear structures under various orientations and widths.

Different types of zero mean filters can be used for curvilinear structure enhancement. The constraint of zero mean will yield zero response on constant structures. For this reason, the proposed filters were enforced to be zero mean, being able at the same time to model a line of specific orientation and width. Figs. 5 and 6 illustrate three of the filters (Step, polynomial, and Gabor filter) that were used for curvilinear structures enhancement. Let $\mathbf{F}(\mathbf{a}, \mathbf{w})$ be a zero mean filter of orientation angle $\mathbf{a}$ and width $\mathbf{w}$.

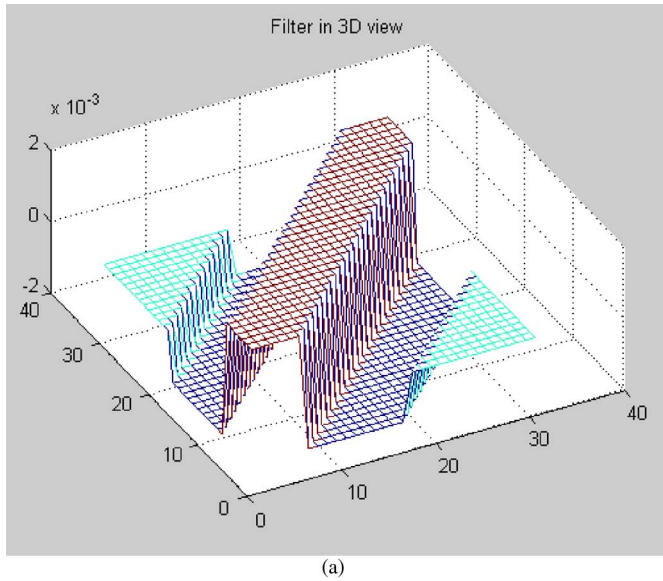

Fig. 5. Three-dimensional view of the step and polynomial filters with a $= 45°$. (a) Step filter. (b) Polynomial filter.

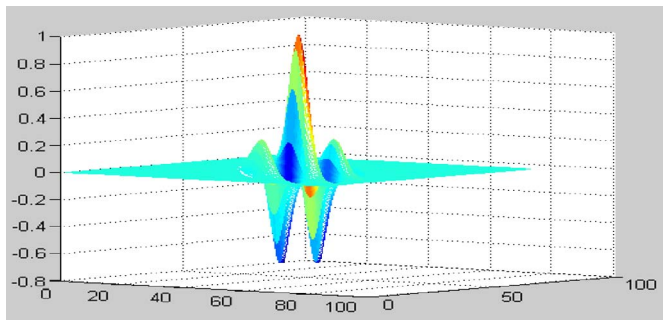

Fig. 6. Three-dimensional view of a Gabor filter.

The step filter $\mathbf{F_s}(\mathbf{a}, \mathbf{w})$ is a simple line model that is given by the extension of one dimension filter $F_s^1(x)$ [see (1)] of width $\mathbf{w}$ in 2-D rotated by $\mathbf{a}$ degrees [see Fig. 5(a)]. The constant c_s is a negative number close to -0.5, estimated by the constraint that the 2-D filter is zero mean. The methodology for c_s estimation is described in the Appendix

$$F_s^1(x) = \begin{cases} 1, & |x| < w \\ c_s, & w \le |x| < r \cdot w \\ 0, & |x| \ge r \cdot w. \end{cases} \tag{1}$$

The polynomial filter $\mathbf{F_p}(\mathbf{a}, \mathbf{w})$ is a smoothed line model that is given by the extension of one dimension filter $F_p^1(x)$ [see (2)] of width $\mathbf{w}$ in 2-D rotated by $\mathbf{a}$ degrees [see Fig. 5(b)]. The constant c_p is a positive number close to 0.5, estimated by the constraint that the 2-D filter is zero mean. The methodology of c_p estimation is the quite similar with the methodology of c_s estimation (see Appendix section).

$$F_p^1(x) = \begin{cases} 1 - \left(\frac{x}{w}\right)^2, & |x| < w \\ c_p \cdot \left(\left(\frac{x}{w} - 2\right)^2 - 1\right), & w \le |x| < r \cdot w \\ 0, & |x| \ge r \cdot w. \end{cases} \tag{2}$$

In both cases, the filters are normalized to have total energy equal to one. Thus, the filter responses of different angles and widths can be comparable. This property is used in (4). Both step and polynomial filters model and enhance efficiently curvilinear structures. The parameter $\mathbf{r}$ in (1) and (2), which should be greater than one, has been selected to be two in our experiments, yielding the highest performance results.

Alternatively, Gabor filter model [7] can be used (see Fig. 6), since orientation and width are also given as parameters for the filter construction. However, experiments that were carried out with real and synthetic data indicated that Gabor filters cannot enhance curvilinear structures as well as the polynomial or step filters. This is due to the more than one local maximum of a Gabor filter in the vertical direction of the filter orientation, which is not true in line models, making them more efficient for texture analysis and feature extraction applications.

C. Multiple Filtering

Let $\mathbf{F}(\mathbf{a}, \mathbf{w})$ be a zero mean filter of orientation angle $\mathbf{a}$ and width $\mathbf{w}$, described in the previous section. According to the proposed method, we estimate the absolute-value image of the convolution of $\mathbf{I_d}$ with the $\mathbf{F}(\mathbf{a}, \mathbf{w})$ for different angles $\mathbf{a}$ and widths $\mathbf{w}$, getting the images $\mathbf{I_f}(\mathbf{a}, \mathbf{w})$ [see (3)]

$$I_f(a, w) = |I_d * F(a, w)|. \tag{3}$$

Image $\mathbf{I_f}(\mathbf{a}, \mathbf{w})$ hosts an enhancement of the curvilinear structures of orientation $\mathbf{a}$ and width $\mathbf{w}$. The use of absolute value takes into account the fact that curvilinear structures can be appeared in $\mathbf{I_d}$ in local minima or local maxima regions, enhancing both cases. Fig. 7(a) shows the original image. Fig. 7(b) and (c) illustrate $\mathbf{I_{fs}}(\mathbf{90^\circ}, \mathbf{2})$ (step filter response) and $\mathbf{I_{fp}}(\mathbf{90^\circ}, \mathbf{2})$ (polynomial filter response), where vertical lines have been enhanced.

In the proposed scheme, 12 different angles (15° angle step) and two or three different widths were employed, depending on the input data. Finally, the resulting image I_m is provided by getting the maximum of the corresponding pixel values of images $I_f(a, w)$ [see (4)]

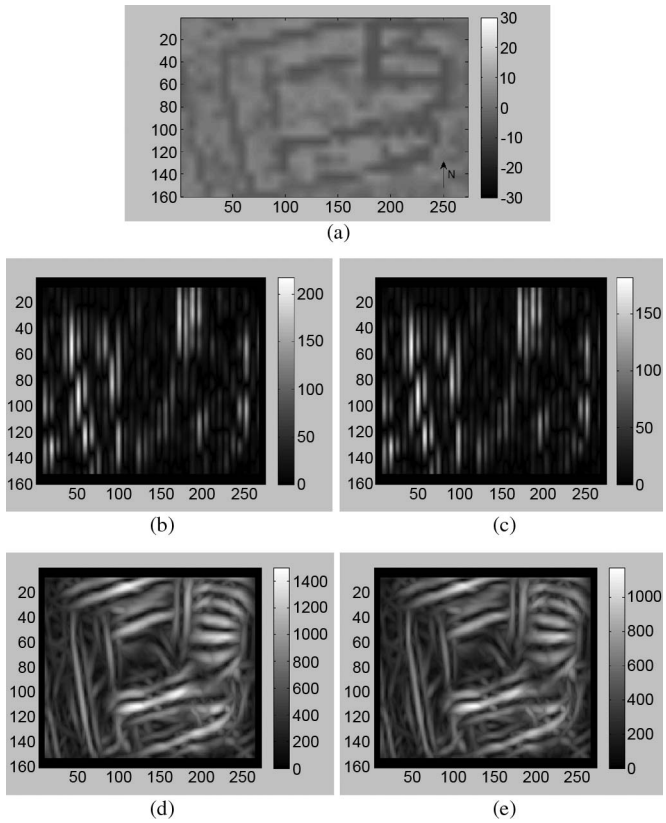

Fig. 7. Results of multiple filtering. (a) Original image (units nT/m). (b) $\mathbf{I_{fs}}(\mathbf{90^\circ}, \mathbf{2})$. (c) $\mathbf{I_{fp}}(\mathbf{90^\circ}, \mathbf{2})$. (d) $\mathbf{I_m}$ for step filters. (e) $\mathbf{I_m}$ for polynomial filters.

$$I_m = \max_{a,w} I_f(a, w). \tag{4}$$

In the resulting image I_m, all curvilinear structures under any orientation have been enhanced. The selection of small-angle step and small changes in widths ensure continuity in I_m. Fig. 7(d) and (e) illustrate an example of $\mathbf{I_m}$ estimation for step and polynomial filtering, respectively. In both cases, two different widths (2 and 4), depending on the width of the expected subsurface structures, and 12 different orientations (15° angle step) were used, resulting in a good curvilinear structure enhancement in any orientation. It holds that the response $\mathbf{I_m}$ using polynomial filtering is smoother with better "balanced enhancement" than the response $\mathbf{I_m}$ using step filtering.

D. Pixel Labeling

The preliminary goal of initial pixel-labeling method is to classify $\mathbf{I_m}$ pixels into three classes C_1, C_2, and C_3 with label numbers 1, 2, and 3, respectively:

- C_1: The pixels that (surely) belong to curvilinear structures.
- C_2: The pixels that we are uncertain if they belong to curvilinear structures.
- C_3: The pixels that (surely) do not belong to curvilinear structures.

The proposed classification is inspired by hysterisis thresholding technique [24]. Hysterisis thresholding has been successfully used on edge detection problem (Canny edge detector [24]). According to hysterisis thresholding, two thresholds $\mathbf{T_l}$ (low) and $\mathbf{T_h}$ (high) are used for initial classification (three classes). A pixel is detected if it is either greater than $\mathbf{T_h}$ (or greater than $\mathbf{T_l}$ and connected to a pixel that is greater than $\mathbf{T_h}$). The advantage of this type of thresholding is that it allows the abstention of some connected point groups [25].

In the proposed scheme, the thresholds $\mathbf{T_l}$ and $\mathbf{T_h}$ are automatically estimated. Let $\mathbf{Med}$ to denote the median value of $\mathbf{I_m}$. Then, $\mathbf{T_l}$ is given by the mean value of $\mathbf{I_m}$ pixels that have a value lower than $\mathbf{Med}$. $\mathbf{T_h}$ is given by the mean value of $\mathbf{I_m}$ pixels that have a value higher than $\mathbf{Med}$. Let $\mathbf{B_i}$ be the image of pixel's initial classification into classes C_1, C_2, and C_3. Let $\mathbf{I_m(p)}$ and $\mathbf{m}$ to denote the value of image $\mathbf{I_m}$ on pixel $\mathbf{p}$ and the median value of nine pixel neighborhood of pixel $\mathbf{p}$ in $\mathbf{I_m}$, respectively.

Then, if $\mathbf{I_m(p)} \geq \mathbf{T_h}$ and $\mathbf{I_m(p)} > \mathbf{m}$, $\mathbf{p}$ is classified to C_1, since its value is very high comparing with the image $(\mathbf{I_m(p)} \geq \mathbf{T_h})$ and with its neighborhood $(\mathbf{I_m(p)} > \mathbf{m})$. If $\mathbf{I_m(p)} \geq \mathbf{T_h}$ or $\mathbf{I_m(p)} > \mathbf{T_l}$ and $\mathbf{I_m(p)} > \mathbf{m}$, $\mathbf{p}$ is classified to C_2 class. If the pixel value is high compared with the image, but it is not high enough compared with its neighborhood or reversely, then it is labeled to an unknown class. Otherwise, $\mathbf{p}$ is classified to C_3 class. The algorithmic steps of the method are given hereafter.

Algorithm **Initial Pixel Labeling**

Input: $\mathbf{I_m}$, $\mathbf{T_l}$, $\mathbf{T_h}$
Output: $\mathbf{B_i}$

```
01: for each pixel p of image I_m
02:   V = set of pixel values of p neighborhood //9 values
03:   m = median(V);              //Median value of V
04:   if I_m(p) ≥ T_h && I_m(p) > m
05:     B_i(p) = 1;
06:   else if I_m(p) ≥ T_h || (I_m(p) > T_l && I_m(p) > m)
07:     B_i(p) = 2;
08:   else
09:     B_i(p) = 3;
10:   end
11: end
```

Finally, a region-growing-based method is executed providing the final pixel labeling into classes C_1 and C_3. So, the goal of this method is to classify the pixels of class C_2. Let $\mathbf{B_f}$ be the image of final pixel classification into classes C_1 and C_3. According to the method, the pixels of C_2 class are classified to C_1 if they are connected to a pixel of C_1, otherwise they are classified to C_3 class.

Thin curvilinear structure detection $(\mathbf{B_t})$ is provided if we change the rule of classification to class C_2 of line 06 of initial pixel-labeling algorithm, removing the case of $\mathbf{I_m(p)} \geq \mathbf{T_h}$.

Fig. 8 illustrates the results of the pixel-labeling method, using as input the geophysical image of Fig. 8(a). $\mathbf{I_m}$ response using polynomial filters is shown in Fig. 8(b). The initial and the final pixel-labeling results are illustrated in Fig. 8(c) and (d), respectively. The white, gray, and black pixels correspond to classes C_1, C_2, and C_3, respectively. Finally, Fig. 8(e) indicates the outcome of the thin curvilinear structure detection, projected on original image Fig. 8(a), with color lines. The color of lines is related to the curvilinear structure enhancement image $\mathbf{I_m}$ (red for high values and blue for low values). The method sufficiently recognizes all curvilinear structures under various orientations and scales.

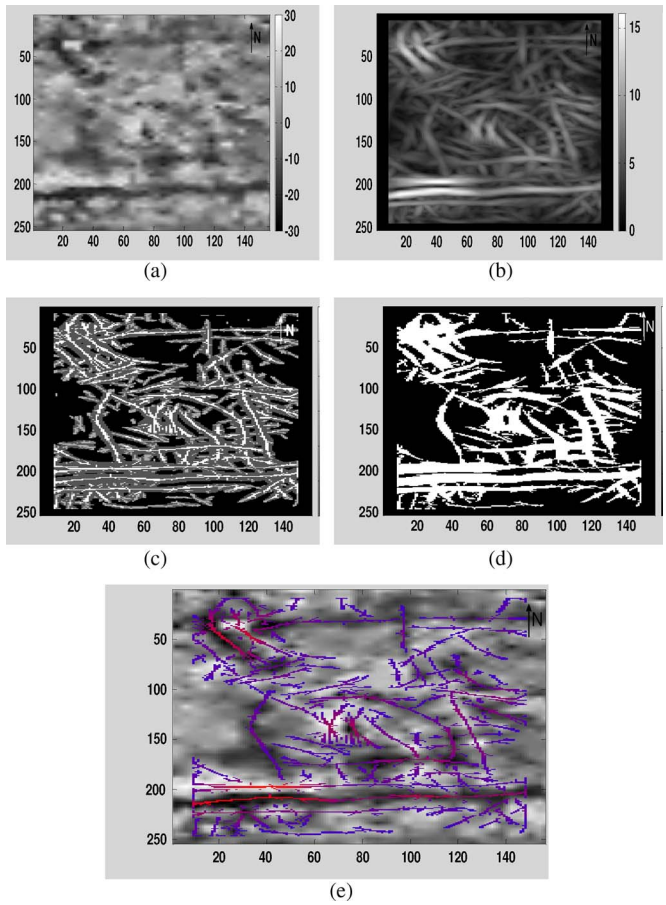

Fig. 8. Results of the pixel labeling. (a) Original image. (b) $\mathbf{I_m}$, curvilinear structure enhancement. (c) $\mathbf{B_i}$, initial pixel labeling (d) $\mathbf{B_f}$, final pixel labeling. (e) $\mathbf{B_t}$, thin curvilinear structure detection.

IV. Experimental Results

In this section, the experimental results of the proposed method, together with comparisons to other schemes and to noise effects, are presented.

A. Description of Experimental Setup

In order to evaluate the proposed method, a database was created, containing digital images, resulting from geophysical mapping in archaeological sites [26] or in areas with geotechnical problems in Greece. Goal of the near-surface geophysical prospecting is mapping the subsurface architectural relics or the detection of features (such as fault zones, karstic voids, etc.) that cause geotechnical problems either to modern structures or ancient monuments. A number of different data sets were

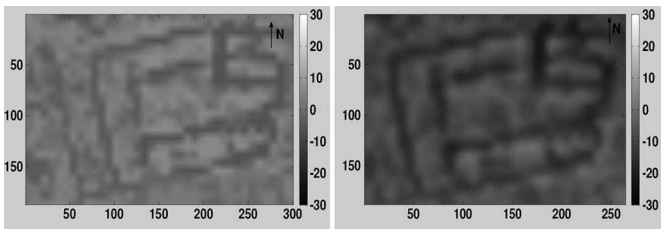

Fig. 9. Original image (left) subjected to RTP (right).

selected in order to test the efficiency of the proposed method. These included high-resolution (0.5 m or 1 m) measurements of the vertical magnetic gradient with a Geoscan FM256 fluxgate gradiometer and electromagnetic measurements acquired by a Geonics EM31 conductivity meter. It has to be mentioned that the method can also be applied to other similar data sets, such as maps resulting from soil resistivity or GPR surveying.

The method was implemented using Matlab and the module-based implementation is illustrated in Fig. 3. For our experiments, we used a Core 2 Duo laptop at 1.5 GHz. The computational complexity of the proposed scheme is $\mathrm{O(N \bullet M)}$, where N denotes the number of pixels in the given image and M the number of filters. A typical processing time for the execution of the proposed scheme is about 15 s for a typical image of 0.25 MP (500×500) and 24 filters.

B. Results of the Proposed Scheme

In order to measure the stability of our method to noise effects, we have added Gaussian white noise to original geophysical images of different signal-to-noise ratio (SNR) levels. The accuracy of pixel- labeling method was measured using the intersection/union metric, defined as the number of correctly detected pixels divided by the number of pixels detected in either the ground-truth labeling or the inferred labeling. This metric has been successfully used to measure image segmentation accuracy [27].

Before applying the proposed scheme, a signal rectification technique can be applied. Reduction to the pole (RTP) is a way for rectifying the magnetic anomalies [28]. RTP converts magnetic anomaly to a symmetrical pattern which would have been observed with vertical magnetization. Fig. 9 illustrates magnetic data subjected to RTP using the software package MagPick v.3 (courtesy of Geometrics Inc.). The IGRF model of 2006 was used in order to specify the magnetic parameters of the regional Earth's magnetic field (for $\lambda = 22^\circ$, $\varphi = 37^\circ$, elevation 144 m) using magnetic field inclination $\mathrm{I} = 53.08^\circ$, magnetic field declination $\mathrm{D} = 2.99^\circ$, and total field intensity $\mathrm{T} = 45109.12$ nT. Only induced magnetization was considered. Hereafter, in order to show the robustness of the proposed scheme to magnetic anomalies, we have not used any signal rectification technique.

Fig. 10 illustrates results of the pixel-labeling method projected on an original geophysical image [see Fig. 10(a)] that was used as input. The particular data came from a magnetic survey combined with other geophysical methods in the ancient site of Sikyon and indicates the presence of a Byzantine Basilica [29] with various linear and curvilinear structural details.

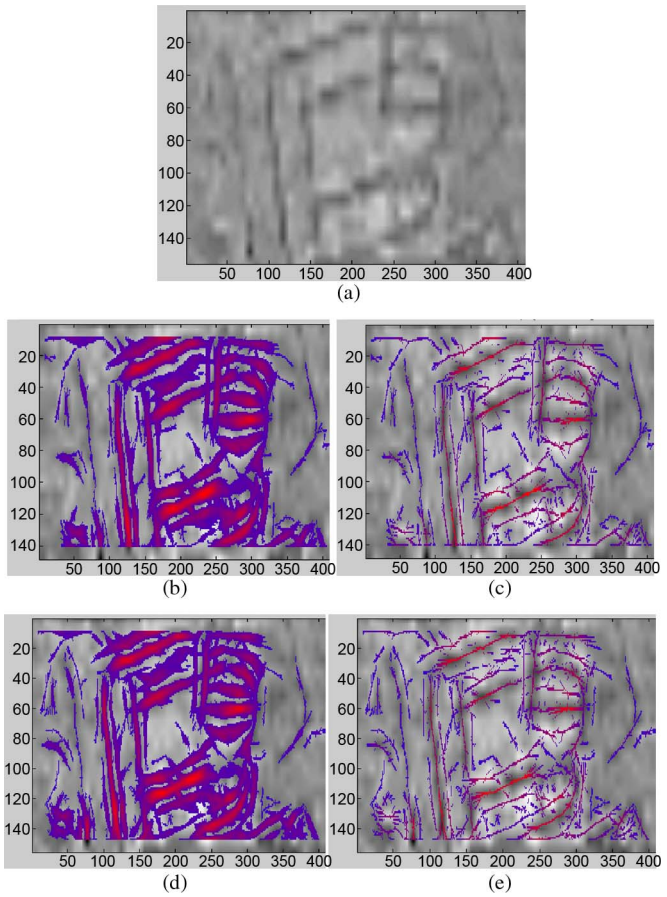

Fig. 10. Results of pixel-labeling method projected on original image. Direction of north is the same as in Fig. 9. (a) Original image. (b) Final pixel labeling (step filters). (c) Thin curvilinear structure detection (step filters). (d) Final pixel labeling. (e) Thin curvilinear structure (polynomial filters) detection (polynomial filters).

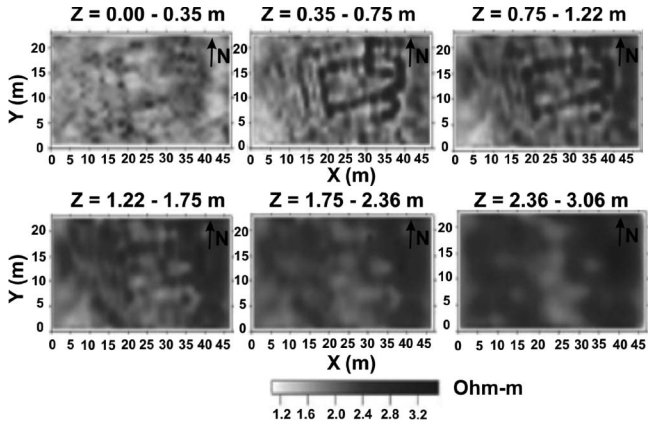

Fig. 11. Three-dimensional resistivity model of the Agora basilica resulting from the 3-D inversion of dipole-dipole parallel electrical resistivity tomographies carried out with Syscal Pro ERT unit. The %RMS error out of nine iterations is 4.5%.

The Basilica presents an inner and outer narthex, dated perhaps from the early Byzantine, and geophysical investigations indicated that it has at least two different construction phases that extend 1.5 m below the surface. More specific information regarding the stratigraphy of the monument was obtained by ERT (dipole-dipole configuration of electrodes) (see Fig. 11)

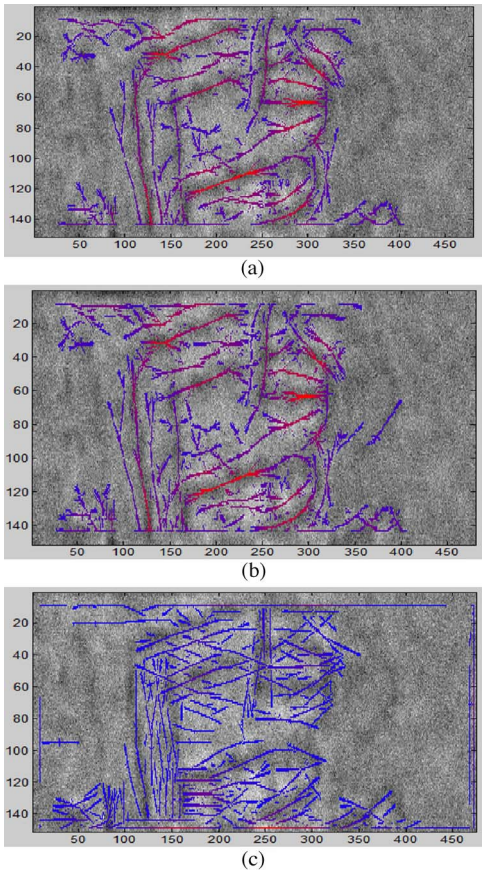

Fig. 12. Results of pixel-labeling method and other techniques projected on original noisy image. Direction of north is the same as in Fig. 9. (a) Thin curvilinear structure detection using step filters. (b) Thin curvilinear structure detection using polynomial filters. (c) Thin curvilinear structure detection using Gabor filters.

and GPR (EKKO 1000) measurements [29]. The non-detected regions are illustrated in grayscale using the original image intensity. The detected regions are colored according to the curvilinear structure enhancement image $\mathbf{I_m}$ (red for high values and blue for low values), providing at the same time the proposed curvilinear enhancement results (weak and strong detections). Therefore, the strong curvilinear structures detections are colored with red color, while the weak detections are colored with blue color. Similarly, Fig. 12 illustrates the results of the pixel-labeling method projected on noisy geophysical image of SNR $= 0.5$ db. In both cases, the proposed method recognized sufficiently the curvilinear structural segments. The employment of polynomial filters seems to offer more details even in the case of noisy geophysical images [see Fig. 12(b)], since the polynomial model is smoother that the step model and fits better on "curved" regions. Step filter fits better on slightly curved features and the Gabor filter seems to highlight the linear segments. In Figs. 10 and 12, the direction of north is the same as in Fig. 9.

Fig. 13 illustrates the intersection/union metric for polynomial and step filters under different SNR for the example of Fig. 10(a). Step filters slightly outperform the polynomial filters. According to this experiment, the intersection/union metric for step filters is about 2.5% higher than the intersection/union metric for polynomial fillers, in average, suggesting that the results are quite similar.

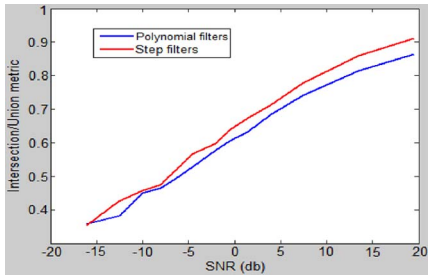

Fig. 13. Intersection/union metric of the two proposed schemes under noise effects of different SNRs for image of Fig. 10(a).

Fig. 15 illustrates the results of pixel-labeling method projected on a synthetic geophysical image [30] that was used as input. The synthetic geophysical image corresponds to the simulated total magnetic field ΔT of a model prism. The prism was placed at a depth of 1 m, having a length and a width equal to 20 m and a depth extension of 2 m. The geomagnetic field inclination was defined as $\mathrm{I}_0 = 5^\circ$ and the declination as $\mathrm{D}_0 = 10^\circ$. Only induced magnetization was considered for the model prism, equal to $\mathrm{J} = 0.35$ A/m. A Gaussian white noise of 5-dB SNR was also added on the data. The color map of this example is similar to the one of Fig. 10. It is shown that the strong detections (red color) under polynomial or step filters correspond to the highest values of the total magnetic field ΔT while some of the weaker detections (illustrated by blue color) are due to the lower values of the magnetic field or noise effects. Therefore, in both cases, the results are quite compatible.

C. Comparisons With Other Methods

To our knowledge, the problem of automatic detection of curvilinear structures in geophysical images from archaeological sites is faced for the first time in this research. So, in order to measure the reliability of the proposed method, a comparison of the proposed scheme with other similar image processing methods like Gabor filtering was carried out. The model of Fig. 6 was employed for the particular experiments, which can be used to model lines under different widths and orientations in a similar way of polynomial and step multiple filtering. Next, the proposed pixel- labeling method was applied (see Fig. 12). Similarly, the pixel-labeling method was compared with hysterisis thresholding technique. The hysterisis thresholding technique gets as input the results of multiple filtering similar to pixel-labeling method. The same thresholds $\mathbf{T_l}$ and $\mathbf{T_h}$ as in the proposed labeling method were used.

The intersection/union metric, presented in the previous section, was used to compare the stability of the proposed scheme and the effect of Gabor filters and hysterisis thresholding technique under different SNRs (Fig. 14). The synthetic data of Fig. 15(a) were used as input in order to have full control of the experiment. It is suggested that the proposed scheme outperforms the rest, yielding the most precise results under low and high levels of Gaussian white noise. Figs. 16 and 17 illustrate curvilinear detection results using as input the synthetic image of Fig. 15(a) adding Gaussian white noise of 45-dB (low level of noise) and 10-dB SNR (high level of noise), respectively.

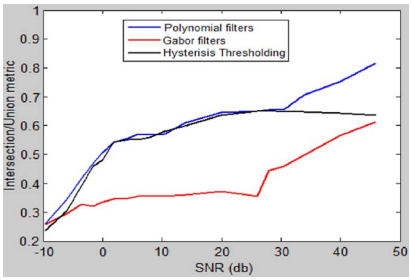

Fig. 14. Intersection/union metric of the proposed scheme (under polynomial filters), Gabor filter and hysterisis thresholding under noise effects of different SNRs.

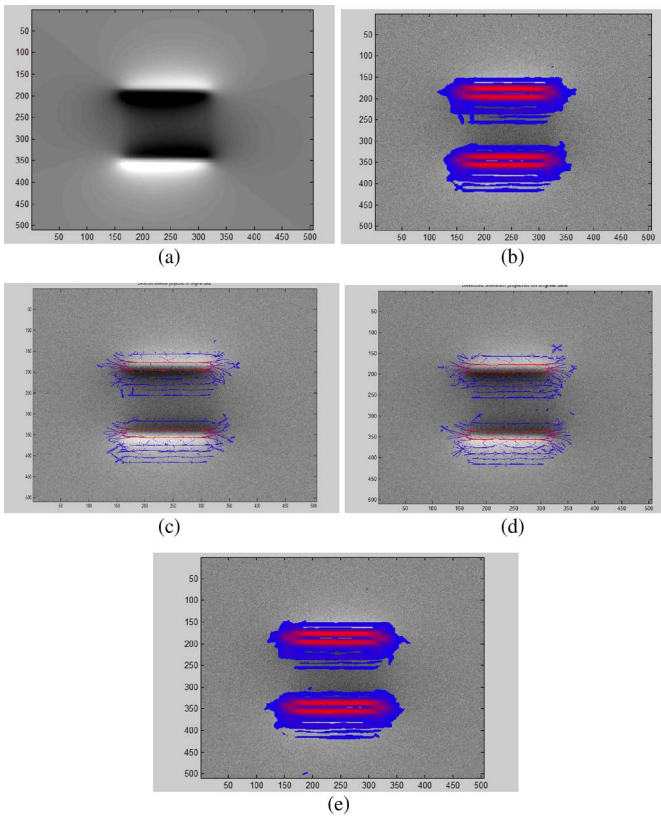

Fig. 15. Results of proposed method on a synthetic noisy geophysical image (SNR $= 5$ db). (a) Original image. (b) Final pixel labeling (step filters). (c) Thin curvilinear structure. (d) Thin curvilinear structure detection (step filters) detection (polynomial filters). (e) Final pixel labeling using step filters.

However, in the case of low-level noise, the detected region using hysterisis thresholding was larger than the ground-truth region, yielding a low accuracy (see Fig. 16). In the case of high-level noise, hysterisis thresholding yielded almost the same results as the proposed method (see Fig. 17). Gabor filters gave the worst results (see Figs. 16 and 17). According to the experimental results in synthetic and real geophysical images, the proposed scheme gave the best results compared to the other two schemes, while the usage of hysterisis thresholding gave similar results under high level of additive noise.

The most significant factor constraining the pixel labeling is the skeleton's sensitivity to an object's boundary deformation, since strong noise sometimes generates redundant skeleton

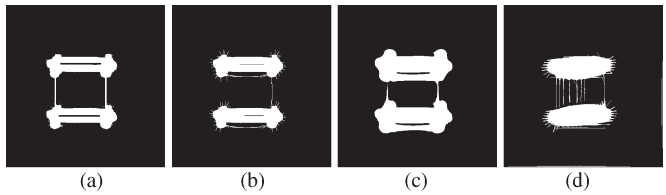

Fig. 16. Curvilinear detection results using as input the synthetic image of Fig. 15(a) adding Gaussian white noise of 45-dB SNR. (a) Ground-truth image. (b) Proposed method detection using polynomial filters. (c) Hysterisis thresholding detection. (d) Gabor filters detection.

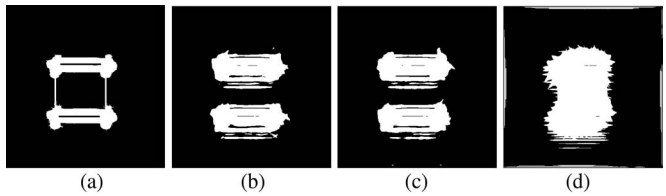

Fig. 17. Curvilinear detection results using as input the synthetic image of Fig. 15(a) adding Gaussian white noise of 10-dB SNR. (a) Ground-truth image. (b) Proposed method detection using polynomial filters. (c) Hysterisis thresholding detection. (d) Gabor filters detection.

branches (false alarms) (e.g., Fig. 8). Due to the proposed method, even bad preserved subsurface structures producing a weak magnetic response, such as the right curved part of Byzantine Basilica in Fig. 10, are well detected.

V. Conclusion

In this paper, a fast, effective, and automatic method for enhancement and detection of partly curvilinear structures in 2-D geophysical images has been proposed. The method has been applied on real and synthetic geophysical images (with low and high levels of noise), recognizing the curvilinear patterns of subsurface architectural structures that exist in archaeological sites. The problem of identification of curvilinear structures in geophysical images for archaeological sites is very difficult due to the interpretation and nature of geophysical images and it is faced for the first time in this research.

The proposed method efficiently combines a rotation- and scale-invariant multiple filter scheme with a pixel-labeling algorithm. In multiple filtering, we have proposed two different filter models, the step and polynomial models. The proposed multiple filtering schemes seem to be effective in curvilinear structure enhancement, giving better results than a Gabor-based filtering scheme. The pixel-labeling algorithm outperforms than hysterisis thresholding technique in curvilinear structure detection. Consecutively, the experimental results, as well as the comparison with alternative techniques in literature, show the satisfactory performance and the robustness of the proposed method in a wide range of geophysical images.

Appendix

First, we estimate the filter for $c_p = 0.5$. Let N_1 and m_1 be the number of points where the filter is positive and their mean value, respectively. Let N_2 and m_2 be the number of points where the filter is negative and their mean value, respectively.

Next, we multiply the negative values of the filter by λ. Then, the mean value of the filter is given by

$$\mathrm{E} = \frac{m_1 \cdot N_1 + \lambda \cdot m_2 \cdot N_2}{N_1 + N_2}.$$

We set $\mathrm{E} = 0$ in order to get a zero mean filter. Thus, λ is given: $\lambda = -(m_1 \cdot N_1)/(m_2 \cdot N_2)$ and $c_p = 0.5 \cdot \lambda$.

ACKNOWLEDGMENT

The authors would like to thank the anonymous reviewers for the critical review and constructive comments.

REFERENCES

[1] P. Hough, "Method and means for recognizing complex patterns," U.S. Patent 3 069 654, Dec. 18, 1962.
[2] N. Aggarwal and W. C. Karl, "Line detection in image through regularized hough transform," *IEEE Trans. Image Process.*, vol. 15, no. 3, pp. 582–591, Mar. 2006.
[3] D. Ioannoua, W. Hudab, and A. F. Laine, "Circle recognition through a 2-D Hough transform and radius histogramming," *Image Vis. Comput.*, vol. 17, no. 1, pp. 15–26, Jan. 1999.
[4] N. Guil and E. L. Zapata, "Lower order circle and ellipse Hough transform," *Pattern Recognit.*, vol. 30, no. 10, pp. 1729–1744, Oct. 1997.
[5] T. M. Koller, G. Gerig, G. Székely, and D. Dettwiler, "Multiscale detection of curvilinear structures in 2-D and 3-D image data," in *Proc. ICCV*, 1995, pp. 864–869.
[6] J.-H. Jang and K.-S. Hong, "Detection of curvilinear structures and reconstruction of their regions in gray-scale images," *Pattern Recognit.*, vol. 35, no. 4, pp. 807–824, Apr. 2002.
[7] J. G. Daugman, "Two-dimensional spectral analysis of cortical receptive field profiles," *Vision Res.*, vol. 20, no. 10, pp. 847–856, 1980.
[8] P. Yang, S. Shan, W. Gao, S. Z. Li, and D. Zhang, "Face recognition using ada-boosted gabor features," in *Proc. Conf. Face Gesture Recog.*, 2004, pp. 356–361.
[9] S. Grigorescu, N. Petkov, and P. Kruizinga, "Comparison of texture features based on Gabor filters," *IEEE Trans. Image Process.*, vol. 11, no. 10, pp. 1160–1167, Oct. 2002.
[10] X. Wang, X. Ding, and C. Liu, "Gabor filters-based feature extraction for character recognition," *Pattern Recognit.*, vol. 38, no. 3, pp. 369–379, Mar. 2005.
[11] C. Kirbas and F. Quek, "A review of vessel extraction techniques and algorithms," *ACM Comput. Surv.*, vol. 36, no. 2, pp. 81–121, Jun. 2004.
[12] C. Panagiotakis, E. Kokinou, and A. Sarris, "Archaeological sites detection from geophysical images based on enhancement of curvilinear patterns," in *Proc. Annu. Conf. Comput. Appl. Quantitative Methods Archaeology (CAA)*, Granada, Spain, 2010.
[13] A. Hoover, V. Kouznetsova, and M. Goldbaum, "Locating blood vessels in retinal images by piecewise threshold probing of a matched filter response," *IEEE Trans. Med. Imag.*, vol. 19, no. 3, pp. 203–210, Mar. 2000.
[14] E. M. Franken, M. A. van Almsick, P. M. J. Rongen, L. M. J. Florack, and B. M. ter Haar Romenij, "An efficient method for tensor voting using steerable filters," in *Proc. ECCV*, vol. 3954, *LNCS*, 2006, pp. 228–240.
[15] G. Papari and N. Petkov, "Adaptive pseudo-dilation for gestalt edge grouping and contour detection," *IEEE Trans. Image Process.*, vol. 17, no. 10, pp. 1950–1962, Oct. 2008.
[16] W. S. Geisler, J. S. Perry, B. J. Super, and D. P. Gallogly, "Edge co-occurrence in natural images predicts contour grouping performance," *Vision Res.*, vol. 41, no. 6, pp. 711–724, Mar. 2001.
[17] F. Admasu and K. Toennies, "Automatic method for correlating horizons across faults in 3-D seismic data," in *Proc. IEEE Conf. Comput. Vis. Pattern Recog.*, Washington, DC, 2004, pp. I-114–I-119.
[18] D. B. Neff, J. R. Grismore, and A. W. Lucas, "Automated seismic fault detection and picking," U.S. Patent 6 018 498, Jan. 25, 2000.
[19] G. Shen and A. Sarris, "Application of wavelet transform in de-noising geophysical data," in *Proc. World Congr. Comput. Sci. Inf. Eng.*, 2009, vol. 6, pp. 223–227.
[20] D. L. Donoho, "De-noising by soft-thresholding," *IEEE Trans. Inf. Theory*, vol. 41, no. 3, pp. 613–627, May 1995.
[21] J. Portilla, V. Strela, M. Wainwright, and E. P. Simoncelli, "Image denoising using scale mixtures of gaussians in the wavelet domain," *IEEE Trans. Image Process.*, vol. 12, no. 11, pp. 1338–1351, Nov. 2003.
[22] T. A. Ridsdill-Smith and M. C. Dentith, "The wavelet transform in aeromagnetic processing," *Geophysics*, vol. 64, no. 4, pp. 1003–1013, Aug. 1999.
[23] B. Tsivouraki and G. N. Tsokas, "Wavelet transform in denoising magnetic archaeological prospecting data," *Archaeol. Prospect.*, vol. 14, no. 2, pp. 130–141, Apr.–Jun. 2007.
[24] J. Canny, "A computational approach to edge detection," *IEEE Trans. Pattern Anal. Mach. Intell.*, vol. 8, no. 6, pp. 679–698, Nov. 1986.
[25] C. D. Kermad and K. Chehdi, "Automatic image segmentation system through iterative edge-region co-operation," *Image Vis. Comput.*, vol. 20, no. 8, pp. 541–555, Jun. 2002.
[26] A. Sarris, S. Topouzi, F. Triantafyllidis, S. Soetens, and G. Pliakou, "Revealing the ancient city of lefkada through the use of shallow-depth geophysical prospection and GIS techniques," in *Proc. 31st CAA Int. Conf.*, 2004, pp. 54–57.
[27] M. Everingham, L. Van Gool, C. K. I. Williams, J. Winn, and A. Zisserman, The PASCAL Visual Object Classes Challenge 2008 Results. [Online]. Available: http://www.pascal-network.org/challenges/
[28] A. H. Ansari and K. Alamdar, "Reduction to the pole of magnetic anomalies using analytic signal," *World Appl. Sci. J.*, vol. 7, no. 4, pp. 405–409, 2009.
[29] A. Sarris, A. N. Papadopoulos, V. Trigkas, E. Kokkinou, E. D. Alexakis, D. Dimitrides, G. Kakoulaki, E. de Marco, E. Seferou, G. Aresti, G. Shen, F. Kondili, M. Karaoulis, M. Karifori, K. Simiridanis, G. Koustas, Y. Nikas-Karayiannis, M. Dogan, G. Stamatis, E. Kappa, Y. Lolos, and T. Kalpaxis, "Recovering the urban network of ancient sikyon through multi-component geophysical approaches," in *Proc. CAA*, 2007, pp. 11–16.
[30] D. Gerovska and M. J. Arauzo-Bravo, "Calculation of magnitude magnetic transforms with high centricity and low dependence on the magnetization vector direction," *Geophysics*, vol. 71, no. 5, pp. 121–130, Sep./Oct. 2006.

Costas Panagiotakis received the B.A, M.Sc., and Ph.D. degrees from the University of Crete, Heraklion, Greece, in 2001, 2003, and 2007, respectively.

He is an Assistant Professor with the Department of Commerce and Marketing, Technological Educational Institute Crete and Visiting Professor in the Department of Computer Science, University of Crete. His interests include video image analysis, pattern recognition, and signal processing.

Eleni Kokinou received the B.A degree from the Aristotelian University of Thessaloniki, Thessaloniki, Greece, in 1993, and the M.Sc. and Ph.D. degrees in geophysics from the Technical University of Crete, Chania, Greece, in 1998 and 2002, respectively.

She is an Assistant Professor with the Department of Natural Resources and Environment of the Technological Educational Institute of Crete, Greece. Her interests include geophysics, geodynamics, signal processing and algorithms.

Apostolos Sarris received the B.A. and M.A. degrees from Boston University, Boston, MA, and the Ph.D. degrees from the University of Nebraska at Lincoln, in 1992.

He is the Director of Research at the Institute for Mediterranean Studies of the Foundation for Research and Technology, Greece and Vice Chairperson of the International Society for Archaeological Prospection. His research is focused on applied geophysics, GIS, satellite remote sensing, and cultural resources management.